Trends in Atmospheric Heat Transport Since 1980

TYLER COX,[a] AARON DONOHOE,[b] KYLE C. ARMOUR,[c,a] DARGAN M. W. FRIERSON,[a] AND GERARD H. ROE[d]

[a] *Department of Atmospheric Sciences, University of Washington*
[b] *Polar Science Center, Applied Physics Laboratory, University of Washington*
[c] *School of Oceanography, University of Washington*
[d] *Department of Earth and Space Sciences, University of Washington, Seattle, Washington*

(Manuscript received 26 June 2023, in final form 12 December 2023, accepted 16 December 2023)

ABSTRACT: We investigate the linear trends in meridional atmospheric heat transport (AHT) since 1980 in atmospheric reanalysis datasets, coupled climate models, and atmosphere-only climate models forced with historical sea surface temperatures. Trends in AHT are decomposed into contributions from three components of circulation: (i) transient eddies, (ii) stationary eddies, and (iii) the mean meridional circulation. All reanalyses and models agree on the pattern of AHT trends in the Southern Ocean, providing confidence in the trends in this region. There are robust increases in transient-eddy AHT magnitude in the Southern Ocean in the reanalyses, which are well replicated by the atmosphere-only models, while coupled models show smaller magnitude trends. This suggests that the pattern of sea surface temperature trends contributes to the transient-eddy AHT trends in this region. In the tropics, we find large differences between mean-meridional circulation AHT trends in models and the reanalyses, which we connect to discrepancies in tropical precipitation trends. In the Northern Hemisphere, we find less evidence of large-scale trends and more uncertainty, but note several regions with mismatches between models and the reanalyses that have dynamical explanations. Throughout this work we find strong compensation between the different components of AHT, most notably in the Southern Ocean where transient-eddy AHT trends are well compensated by trends in the mean-meridional circulation AHT, resulting in relatively small total AHT trends. This highlights the importance of considering AHT changes holistically, rather than each AHT component individually.

KEYWORDS: Dynamics; Hadley circulation; Heat budgets/fluxes; Thermodynamics

1. Introduction

Poleward atmospheric heat transport (AHT) plays a fundamental role in moderating the equator-to-pole temperature gradient and its changes under external forcing. Previous work has pointed out that AHT plays an important role in many observed climate changes including Arctic warming (e.g., Alexeev and Jackson 2013; Hahn et al. 2021) and sea ice loss (e.g., Woods et al. 2013; Woods and Caballero 2016; Kapsch et al. 2013). AHT is also tightly coupled to the hydrologic cycle (e.g., Held and Soden 2006; Pierrehumbert 2010; Siler et al. 2018; Fajber et al. 2023). Given the importance of AHT for Earth's climate, understanding how AHT has changed over the past several decades is an important endeavor.

Climate models predict that AHT will increase in magnitude at most latitudes with global warming, although the changes are expected to be relatively small (less than 5% of climatology) through the end of the twenty-first century (e.g., Hwang and Frierson 2010; Armour et al. 2019; Zelinka and Hartmann 2012). This raises questions of whether a strengthening of the climatological AHT is observable in the past few decades, and whether models have been able to accurately capture the changes.

Previous studies have partially answered these questions by exploring how specific aspects of AHT have changed over the satellite era (since about 1980) using reanalysis datasets, coupled climate models driven by historical forcing, and atmosphere-only models driven by observed sea surface temperatures. This previous work has used a range of methods to calculate AHT or has relied on AHT-adjacent metrics including eddy kinetic energy and mass transports (e.g., Hu et al. 2018; Chemke and Polvani 2019; Zaplotnik et al. 2022; Chemke and Polvani 2020; Shaw et al. 2022). While these metrics are dynamically meaningful, our focus in this work is on the total vertically and zonally integrated AHT, which is closely connected to Earth's energy budget. Following the AHT-calculation methodology of Donohoe et al. (2020), we maintain a definition of AHT that can be related to the energy budget of the atmosphere while decomposing AHT into three dynamic components (e.g., Holton and Staley 1973) to gain insight into compensation between the changes in each component. The three components contributing to AHT are conceptually summarized here:

(i) mean-meridional circulation AHT (MMC) which represents the time- and zonal-mean mass overturning circulation of the atmosphere that transports energy poleward in the tropical Hadley cells and equatorward in the extratropical Ferrel cells.
(ii) stationary eddy AHT (SE) which represents the zonally varying time-mean circulations associated with active storm-track regions.
(iii) transient eddy AHT (TE) which represents the net heat transport by synoptic storms.

Supplemental information related to this paper is available at the Journals Online website: https://doi.org/10.1175/JCLI-D-23-0385.s1.

Corresponding author: Tyler Cox, tylersc@uw.edu

DOI: 10.1175/JCLI-D-23-0385.1

We refer to the eddy component as the sum of TE and SE and provide a more thorough mathematical breakdown of these components in section 2.

Eddy sensible heat fluxes make up one part of the eddy component of AHT. Specifically, eddy sensible heat fluxes include just the sensible heat portion, not the latent or geopotential portions, of the eddy component. There is evidence that, on a hemispheric scale and in the annual mean, these eddy sensible heat fluxes have strengthened in the Southern Hemisphere and weakened in the Northern Hemisphere since 1980 (Chemke and Polvani 2020). This is likely due in part to a strengthening meridional surface air temperature (SAT) gradient in the Southern Hemisphere and a weakening SAT gradient in the Northern Hemisphere (Chemke and Polvani 2020). Both coupled and atmosphere-only models are able to capture the eddy sensible heat flux trend in the Northern Hemisphere, while only atmosphere-only models capture the trend in the Southern Hemisphere (Chemke and Polvani 2020). The inability of coupled models to reproduce the Southern Hemisphere eddy sensible heat fluxes is tied to their inability to accurately capture the observed SAT and sea surface temperature (SST) patterns (Liu et al. 2022; Chung et al. 2022; Dong et al. 2021). However, atmosphere-only models also fail to capture the wintertime eddy AHT trends due to inaccuracies in simulating the zonal-mean circulation (Chemke et al. 2022). Shaw et al. (2022) suggests there may be discrepancies between reanalysis and models in AHT trends in some regions, but primarily focuses on AHT-adjacent metrics. This provides us with a useful starting place for exploring AHT trends, but leaves open the question of how total AHT and each of its components (TE, SE, and MMC) have changed in the annual mean.

It has also been found that in the Northern Hemisphere, SE trends in individual months may be driven more by changes in tropical heating, while TE trends may be driven more by meridional land temperature gradients (Park and Lee 2022). Additionally, compensation between SE and TE trends can be important in some months (Park and Lee 2022). However, this work primarily uses bandpass filtering to identify the TE and SE components and has focused on broad swaths of each hemisphere.

While tropical AHT has not been the primary focus of any previous work, there has been research into tropical mass-transport trends (Hu et al. 2018; Chemke and Polvani 2019; Zaplotnik et al. 2022). This previous work found that reanalysis datasets and models do not agree on Hadley-cell mass transport trends because of errors in the way the reanalyses represent latent heating and precipitation (Hu et al. 2018; Chemke and Polvani 2019; Zaplotnik et al. 2022). While some of the trends in Hadley-cell mass transports in reanalysis datasets may be real, the authors of previous work recommend caution when using reanalysis in the tropics. One aim of this work is to investigate whether these same errors impact AHT trends.

As summarized above, most previous work [with the exception of parts of Park and Lee (2022)] focuses on individual AHT components, primarily TE. Given the extensive literature about connections between AHT components (Walker and Schneider 2006; Branstator 1995; Chang et al. 2002; Donohoe et al. 2020; Cox et al. 2022), as well as the smoothly varying nature of AHT with latitude (Trenberth and Stepaniak 2003), it seems important to consider all AHT components simultaneously, which would afford a more complete picture of how AHT has been changing. The interconnected nature of AHT components also means that assigning cause and effect can prove challenging; a change in one component will cause a change in another component. Additionally, much of this previous work has averaged AHT trends over large swaths in the midlatitudes. While this is convenient, there may be interesting AHT trend variations with latitude that this sort of averaging analysis would miss.

In this work, we aim to provide a comprehensive evaluation of AHT trends in CMIP6 models and three different reanalysis datasets since the beginning of the satellite era (1980). We focus on evaluating all AHT components and compensations between them, providing a more complete picture of how AHT has changed. We also document regions where we have greater or lesser confidence in the trends based on agreement among datasets and physical understanding.

In section 2, we describe the reanalysis datasets and models we use and explain our method for calculating AHT. We then organize our analyses into three main sections, organized by latitude. First, in section 3a, we revisit the Southern Hemisphere midlatitude eddy trends initially explored in Chemke and Polvani (2020) and Chemke et al. (2022) and find that there is general agreement between reanalysis datasets on a strengthening of the climatological TE and MMC, giving us confidence in these trends. We find that atmosphere-only models are generally able to capture the TE trends better than coupled models, and all TE trends are strongly compensated by MMC trends, such that total AHT does not change much. Second, in section 3b, we examine tropical AHT trends and find large discrepancies in MMC trends between reanalysis datasets and models. We find that the spread in MMC trends among the reanalyses and an ensemble of models is well explained by the trends in precipitation. Third, in section 3c, we examine Northern Hemisphere midlatitude AHT trends, which are generally smaller and in less agreement among reanalysis datasets and models than trends in the Southern Hemisphere midlatitudes leading to lower confidence in the trends. We find agreement among reanalysis datasets and models in increases in TE around 50°N, which we link to SST changes, and mismatches between reanalysis datasets and models for AHT trends north of 60°N, which we link to the varying abilities of models to accurately capture Arctic amplification. Last, in section 3d, we examine compensation between trends in different AHT components, which generally results in smaller trends in total AHT than in individual components. Where possible, we explain discrepancies between models and the reanalyses, and provide physical explanations for the largest trends. We also direct most of our focus to annual-mean AHT trends.

2. Methodology and datasets

One aim of this work is to present an analysis of AHT trends using the most state-of-the-art datasets available. We calculate AHT for the ERA5 (Hersbach et al. 2020), JRA-55 (Kobayashi et al. 2015), and MERRA-2 (Gelaro et al. 2017)

datasets as these are all regularly updated through the present day.

We use a variety of simulations to assess how well climate models have predicted AHT trends over the satellite era. We use historical simulations of 31 fully coupled climate models participating in phase 6 of the Coupled Model Intercomparison Project (CMIP6; Eyring et al. 2016). We also use 28 atmosphere-only simulations [following the Atmospheric Model Intercomparison Project (AMIP); Hurrell et al. 2008] driven by SSTs and sea ice concentrations prescribed to match the historical record performed as part CMIP6 (Eyring et al. 2016). The list of models and experiment names used in this work can be found in Table 1 in the online supplemental material. We use the "r1i1p1f1" ensemble member for all models.

We present results from 1980 through 2014 as this is the period of time in which all data sources have data available (AMIP simulations end in 2014). Using data through 2022 for sources where it is available (reanalyses and coupled models) does not impact the general conclusions.

In addition to 31 coupled models and 28 AMIP models, we also calculate AHT trends for three historical ensembles of NCAR's CESM2 (Danabasoglu et al. 2020). The first is the 100-member CESM2-LENS2 ensemble (Rodgers et al. 2021). The other two are the 10-member CESM2-GOGA ensemble, which is a global-AMIP simulation, and the 10-member CESM2-TOGA ensemble, which is a tropical-AMIP simulation in which tropical SSTs are prescribed to match the observations while extratropical SSTs are set to climatology.

We calculate AHT for each month using the methodology of Donohoe et al. (2020), which we describe briefly below. AHT is defined at each latitude (θ) as

$$\mathrm{AHT}(\theta) = \frac{2\pi a \cos(\theta)}{g} \int_0^{\overline{P_s}} \Big(\underbrace{[\overline{v}]^{\dagger}[\overline{\mathrm{MSE}}]^{\dagger}}_{\mathrm{MMC}} + \underbrace{[\overline{v^*}\ \overline{\mathrm{MSE}^*}]}_{\mathrm{SE}} + \underbrace{\overline{[v^{*\prime}\mathrm{MSE}^{*\prime}]}}_{\mathrm{Transients}} + \overline{[v]'[\mathrm{MSE}]'} \Big) dp, \tag{1}$$

where v is the meridional wind, MSE is the moist-static energy, p is pressure, $\overline{P_s}$ is the climatological surface pressure, a is the radius of Earth, square brackets [ ] denote zonal averages, overbars ($\overline{X}$) denote monthly time averages, asterisks (*) are departures from the zonal average, primes ($'$) are departures from the monthly time average, and daggers (†) are departures from the vertical average. We remove the vertical averages from both terms in the MMC to account for possible lack of mass conservation.

The MMC and SE portions of the AHT can be computed from monthly-mean data. However, the transients portion of the AHT requires the covariance of v and MSE at 6-hourly time scales. This presents difficulties as not all CMIP6 models make the needed 6-hourly data easily available, and even if they were available, it would involve hundreds of terabytes of data. Donohoe et al. (2020) provide a novel workaround for this problem by calculating the total AHT in each month using surface and top-of-atmosphere fluxes, and then calculating the transients piece as a residual term. While this avoids needing to use 6-hourly data to calculate the transients component, it does require accurate estimates of surface heat fluxes and a closed atmospheric energy budget. In models, the surface fluxes are known and are internally consistent with the atmospheric energy budget and atmospheric dynamics. However, atmospheric reanalyses generally do not conserve energy and provide surface flux data that are not directly constrained by observations (Chaudhuri et al. 2013; Trenberth et al. 2009; Wild et al. 2013, 2015). We thus calculate the transients AHT component for the reanalyses directly using 6-hourly data. Donohoe et al. (2020) find excellent agreement between these two calculation methodologies when tested within a climate model where 6-hourly fields were available.

The transients AHT component includes contributions from both transient eddies (first term in the transients) and the transient overturning circulation [second term in the transients, termed the TOC in Marshall et al. (2014)]. The TOC term is generally two orders of magnitude smaller than the transient-eddy term (e.g., Marshall et al. 2014; Donohoe et al. 2020). Therefore, we will refer to the Transients term as the TE, even though it does include contributions from both the TE and TOC.

All trends are calculated as the slope of the linear regression of the annual-mean AHT against time and are expressed as the trend per 40 years. While there are indications of interesting nonlinear changes in AHT since 1980, exploring all of these nonlinear AHT changes is beyond the scope of this work. We calculate the standard error of the linear regression coefficients to find the uncertainty in the trends and use a two-sided Student's t test to assess if trends are significantly different from zero.

3. Results

We first consider the mean AHT trends across all three reanalysis datasets, the 28 AMIP models, and the 31 coupled models (Fig. 1). There are large MMC and TE trends over the Southern Ocean (roughly 65°–30°S) with broad agreement between reanalysis datasets and models. In section 3a, we explore the drivers of these Southern Ocean AHT trends. The largest AHT trends of any reanalysis dataset are found in the tropics (Figs. 1a,b). However, in section 3b, we show that the large discrepancy between models and the reanalyses in this region casts doubt on the validity of trends in the reanalyses. The AHT trends in the Northern Hemisphere show less agreement between reanalysis datasets and models than the Southern Ocean trends, leading to less confidence in trends in this region (Fig. 1). However, in section 3c we do find some common drivers of the trends across all reanalysis datasets and models in the Northern Hemisphere.

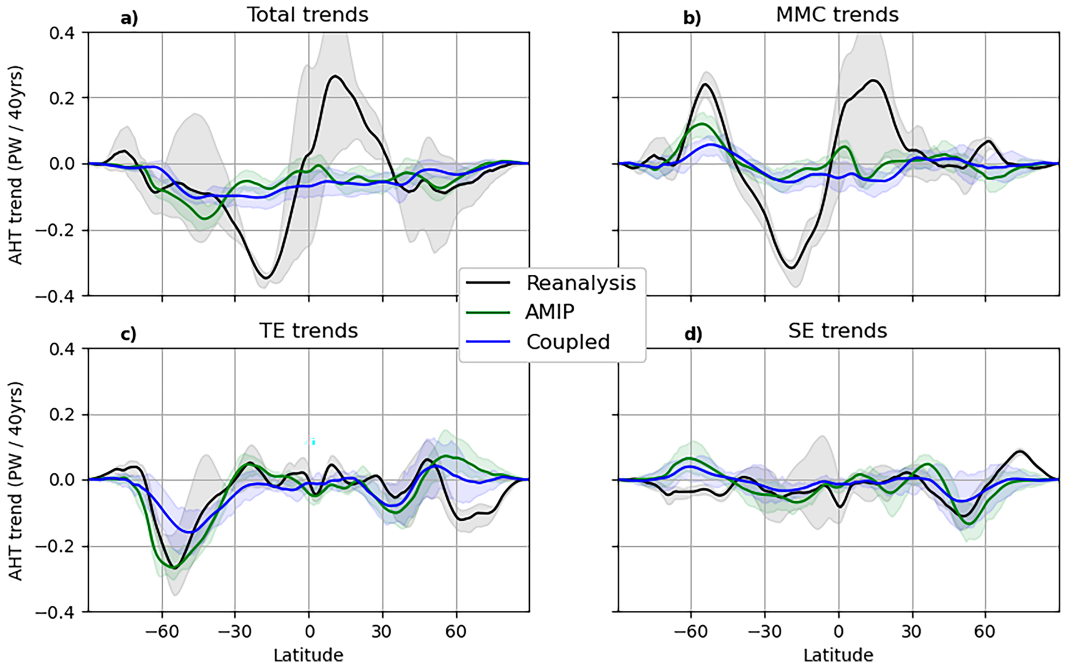

FIG. 1. Mean AHT trends for the 3 reanalyses, 28 AMIP models, and 31 coupled models for the (a) total AHT trends, (b) MMC trends, (c) TE trends, and (d) SE trends. The shading around the AMIP and coupled lines shows the interquartile range, while the shading around the reanalysis lines shows the range across the three reanalyses.

a. *Southern Ocean AHT trends*

In the Southern Ocean, total AHT trends (Fig. 1a) are generally under 0.2 PW (40 years)$^{-1}$ in the ensemble means and agree well between reanalysis datasets and models. A change in total AHT of 0.2 PW at 40°S corresponds to roughly 5% of the climatology there. The Southern Ocean trends in TE and MMC are each larger in magnitude than the total AHT trends (Figs. 1b,c), but with differing signs for each component, indicating a compensation between them, which tends to limit trends in total AHT. Specific compensation mechanisms will be elaborated on in section 3d. SE trends are smaller (Fig. 1d).

The Southern Ocean trends in TE and MMC are the same sign among reanalysis datasets, the ensemble mean of the coupled models, and the ensemble mean of the AMIP models and are indicative of a strengthening of climatology, with more poleward TE associated with strengthened storms and more equatorward MMC associated with a strengthened Ferrel cell. The AMIP ensemble mean shows similar TE trends to those in the reanalyses, while the coupled ensemble mean predicts smaller TE trends.

In the Southern Ocean, there is good agreement in TE trends between two of the three reanalysis datasets (ERA5 and JRA-55), with MERRA-2 being an outlier showing small TE trends (Fig. 2c). There is considerable intermodel spread in trends in AHT and in each of its components (Fig. 2). AMIP models tend to estimate TE trends that are close to ERA5 and JRA-55, while coupled models produce smaller magnitude TE trends. Coupled models may fail to simulate the observed TE trends because they fail to properly simulate SST trends in the Southern Ocean (Liu et al. 2022; Chung et al. 2022; Dong et al. 2021; Wills et al. 2022). Connections between meridional SST gradients and TE have a wealth of support in the literature (e.g., Held 1999). The relationship between trends in the SST gradient across the Southern Ocean and trends in Southern Ocean TE for the reanalysis datasets, coupled models, and CESM2-LENS2 is shown in Fig. 3. The coupled models fail to reproduce the observed trend in meridional SST gradient (data from ERSSTv5; Huang et al. 2017), and therefore it is not surprising that they also fail to reproduce TE trends from reanalysis datasets. This is also consistent with the work of Chemke and Polvani (2020) that found AMIP models did better than coupled models at reproducing the eddy sensible heat flux trends (rather than AHT trends as in this work) in the reanalyses.

We note that even among the AMIP models, which are forced by observed SSTs, there is still a range of TE trends (Fig. 3, gray violin plot) and not all AMIP models match the TE trends found in the reanalyses. We hypothesize that the differences in AMIP TE trends may be related to their representations of SE trends in the Southern Ocean, which are generally positive in the AMIP simulations and negative in the reanalyses. In particular, SE trends can induce an opposite-signed TE trend due to compensation between these AHT components (section 3d). Indeed, we find a relationship between SE and TE trends in this region within models (see Fig. 1 in the online supplemental material), suggesting that even if an AMIP model accurately captures the TE response to SST trends, it may produce the wrong TE trend if its SE trend is in error. In addition, the AMIP models may be inaccurately capturing the TE response to SST trends leading to the discrepancy between reanalysis and AMIP models TE

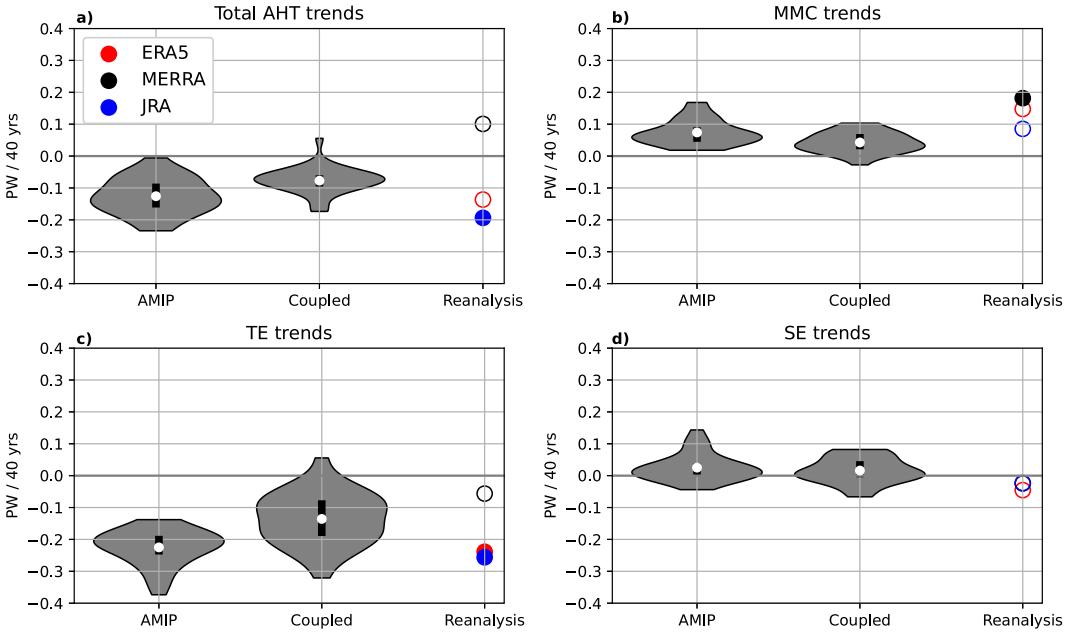

FIG. 2. Trends averaged from 40° to 60°S for (a) total AHT trends, (b) MMC trends, (c) TE trends, and (d) SE trends. For AMIP and coupled models the violin plots show the ensemble distributions, where the width of the shading indicates probability density, the thick black lines indicate the interquartile range, and the white dots indicate the mean value. For the reanalyses, filled circles denote trends that are statistically different from zero at the 95% confidence level, while open circles denote trends that are not.

trends in the Southern Ocean. Last, some of the spread in AMIP models may be coming from internal variability rather than inherent issues with the AMIP models.

SE trends are smaller than TE trends and disagree on sign between the reanalyses and models (Fig. 1d). SE trends agree well among the reanalyses but are outside the range of most, but not all, AMIP and coupled models (Fig. 2d). While the SE trends in this region are small compared to the TE and MMC trends, we propose two possible SE-trend sources in this region: ozone hole–induced changes and tropical SST–induced changes. Ozone depletion has led to stratospheric cooling and shifts in the stratospheric and tropospheric winds in October and November (e.g., Ramaswamy et al. 1996; Randel and Wu 1999; Thompson and Solomon 2002). The ozone hole is not centered over the South Pole and is instead offset toward the Atlantic Ocean during October and November (e.g., Grytsai et al. 2007). This asymmetry induces zonally asymmetric changes, which have led to a strengthening of the climatological eddy heat flux that makes up one part of the eddy AHT (e.g., Ivanciu et al. 2021). Differences in how models simulate stratospheric chemistry have been shown to impact eddy heat fluxes in the Southern Hemisphere, with interactive chemistry models simulating changes more in line with reanalysis and observations (Ivanciu et al. 2021). We find similar results, with models that have interactive stratospheric chemistry capturing the SE trends in the reanalyses during October and November better than those without interactive chemistry (supplemental Fig. 2). This suggests that some of the reanalysis and model SE-trend discrepancy may come from some models inaccurately simulating the ozone hole and ozone hole–induced trends. While this may explain some of the reanalysis and model SE-trend discrepancy during October and November, it does not explain the existence of SE trends during other months of the year.

The second source potential of SE trends are due to tropical SST trends. This is supported by observational and theoretical work (Park and Lee 2019, 2022; Baggett and Lee 2017) that finds tropical heating is linked to SE in the middle and high latitudes. We use the 10-member CESM TOGA ensemble simulations (tropical-only AMIP) and compare them against the 10-member CESM GOGA ensemble simulations (global AMIP) to assess the role of tropical SST trends in driving Southern Ocean SE trends. We find that the Southern Ocean SE trends are similar in both the CESM TOGA and CESM GOGA simulations (supplemental Fig. 3). Because TOGA simulations use climatological SSTs in the extratropics, this suggests the tropical SST trends must be more important than extratropical SST trends for driving the Southern Ocean SE trends. It is not clear if mismatches in tropical SST trends are an additional source of the Southern Ocean SE trend mismatch between reanalysis datasets and models.

We now turn our attention to the MMC trends. On average the MMC trends in the Southern Ocean are slightly larger in AMIP than in coupled models, mirroring slightly larger eddy trends (TE trends plus SE trends) in AMIP than in coupled models (Fig. 2b). Reanalysis MMC trends are mostly beyond the intermodel range for coupled models and near the edge of the range for AMIP models. We further explore compensatory changes between eddies and the MMC in section 3d.

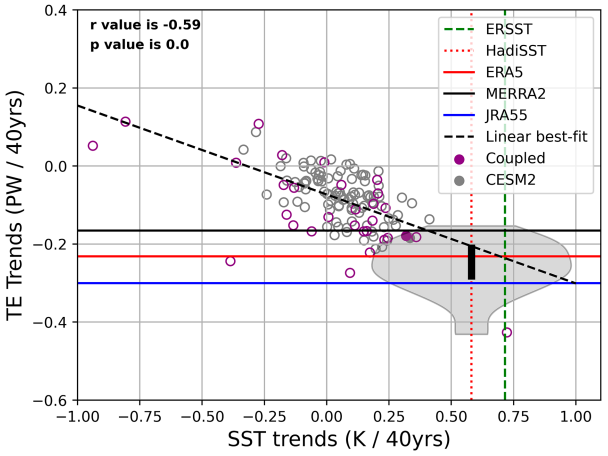

FIG. 3. Trends of SST differences (x axis, the mean from 30° to 50°S minus the mean from 50° to 65°S) vs trends of TE (y axis, the mean from 40° to 60°S) for all three reanalyses, the coupled models, and the CESM2-LENS2. The dashed green vertical line is the ERSSTv5 SST trend estimate (Huang et al. 2017), the dotted red line is the HadISST SST trend estimate (Rayner et al. 2003), the horizontal colored lines are the TE trend estimates from each reanalysis, and the dashed diagonal line is the linear best-fit line with the corresponding correlation coefficient and p value in the top-left corner. AMIP models use the HadISST dataset. Filled circles denote trends that are statistically different from zero at the 95% confidence level, while open circles denote trends that are not. The gray shading of the violin plot shows the AMIP ensemble TE trend values, where the width of the shading indicates probability density and the thick black line indicates the interquartile range.

b. *Tropical AHT trends*

Previous work on tropical Hadley cell trends has cast doubt on the validity of reanalysis datasets in this region (Hu et al. 2018; Chemke and Polvani 2019; Zaplotnik et al. 2022). While this previous work has focused on mass transports in the tropics (rather than AHT), it serves as a reminder that the reanalyses should be interpreted with care and not treated blindly as the "truth" for tropical AHT trends. We find that the largest total AHT trends in the reanalyses come in the tropics, while AMIP and coupled models do not produce large tropical AHT trends (Fig. 1a). Moreover, these trends have been primarily driven by MMC trends, which in the tropics corresponds to Hadley cell trends (Fig. 1b). Trends in the TE and SE components are relatively small.

Focusing on the tropics and subtropics, we find that in the Southern Hemisphere there is relatively good agreement in MMC trends among the reanalyses, but they are outside of the range of AMIP and coupled models (Fig. 4a). In the Northern Hemisphere, we see a similar picture, except that ERA5 suggests an MMC trend near zero, which is in line with those of AMIP and coupled models (Fig. 4b).

The mismatch between models and the reanalyses is also evident in the Hadley-cell mass transports (Fig. 5). The reanalyses show strong agreement in a strengthening of the climatological Hadley cell streamfunctions, AMIP shows a weakening of the Southern Hemisphere Hadley cell but ambiguity in the Northern Hemisphere, and coupled models show good agreement on a minor Northern Hemisphere weakening and some additional minor trends near the equator.

The mismatch in Hadley-cell mass transports between models and the reanalyses has been investigated before and the discrepancies were found to primarily come from issues that the reanalyses have in their representation of latent heating and precipitation (Hu et al. 2018; Chemke and Polvani 2019; Zaplotnik et al. 2022). As this paper is primarily focused on AHT, rather than mass transports, we have not done a thorough examination of Hadley cell trends, for example using the Kuo–Eliassen equation (e.g., Chemke and Polvani 2019). However, we do briefly investigate if the spread in tropical precipitation trends can explain the trends in the MMC by plotting the tropical precipitation trends against the Southern Hemisphere MMC trends (Fig. 6). While these quantities are not necessarily linearly related, we fit a linear best-fit line to all the data points in Fig. 6 and find an r^2 value of 0.56. The strong relationship between tropical precipitation trends and MMC trends suggests that if models and the reanalyses had similar precipitation (and latent heating) trends, they would likely have similar MMC trends as well.

The increase in tropical precipitation is larger in each of the three reanalyses than in any climate-model simulation, or in the more observationally constrained precipitation product from the Global Precipitation Climatology Project (GPCP; Fig. 6; Adler et al. 2003). Previous work has found that producing accurate estimates of tropical precipitation is challenging, with reanalysis datasets performing poorly compared to satellite- and rain gauge–based estimates in many regions (Hassler and Lauer 2021; Sun et al. 2018; Kim and Alexander 2013; Lavers et al. 2022). Altogether, the mismatch between model and reanalysis trends in tropical precipitation and AHT combined with the difficulty of constraining observed tropical precipitation trends, makes it difficult to definitively conclude how tropical AHT has changed since 1980. However, the tropical MMC trends in the reanalyses are very large (nearly 20% of climatology) and are likely unreasonable given the lack of corroborating observational evidence of AHT changes of this magnitude (e.g., the lack of correspondingly large precipitation trends in GPCP data).

c. *Northern Hemisphere AHT trends*

While the Southern Hemisphere middle to high latitudes show clear AHT trends peaking at roughly 55°S, the Northern Hemisphere middle to high latitudes show more latitudinal variations and less agreement between datasets (Fig. 1). The Northern Hemisphere TE and MMC trends are also smaller in magnitude than in the Southern Hemisphere (Fig. 1). We hypothesize that part of this hemispheric discrepancy may be due to hemispheric asymmetries in the meridional pattern of SST changes since 1980. While warming of the Northern Hemisphere SSTs has been most substantial north of 60°N (e.g., Gu et al. 2016), Southern Ocean warming has been largest more equatorward, near 35°S, with cooling farther south (supplemental Fig. 4). This has resulted in a decrease in the meridional SST gradient in the Northern Hemisphere and an increase in the Southern Hemisphere.

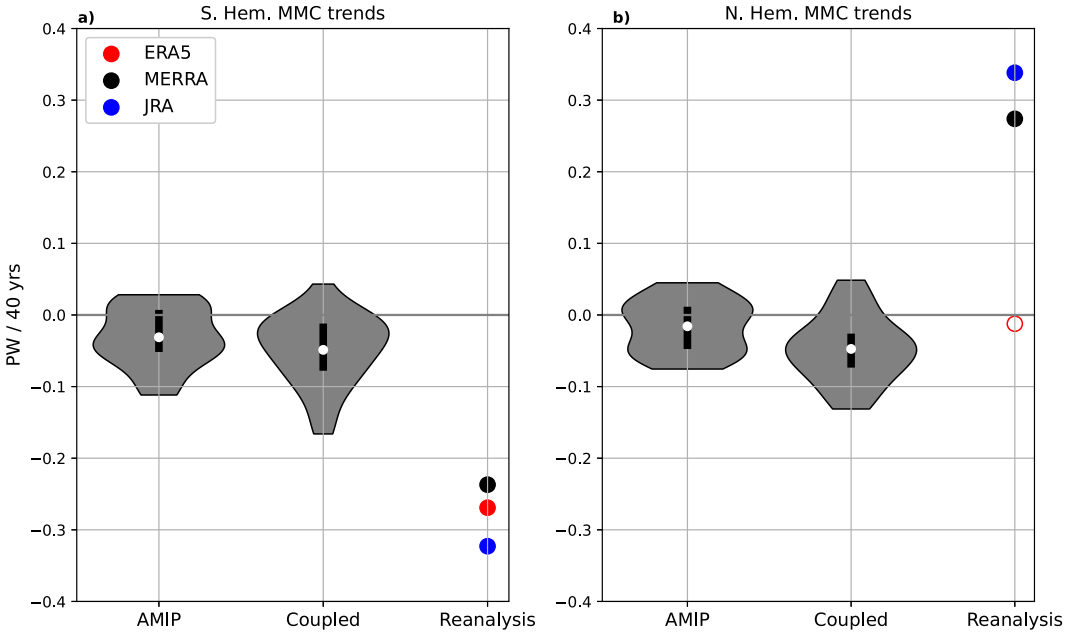

FIG. 4. MMC trends in the (a) Southern Hemisphere tropics averaged from 20° to 25°S and (b) in the Northern Hemisphere tropics averaged from 10° to 25°N. For AMIP and coupled models the violin plots show the ensemble distributions, where the width of the shading indicates probability density, the thick black lines indicate the interquartile range, and the white dots indicate the mean value. For the reanalyses, filled circles denote trends that are statistically different from zero at the 95% confidence level, while open circles denote trends that are not.

We focus on Northern Hemisphere mid- to high-latitude AHT trends in two specific regions that have the largest magnitude AHT trends. The first region is north of 60°N where the mean of the reanalysis datasets shows negative TE trends, while the coupled models mean is close to zero, and the AMIP models mean shows positive TE trends (Fig. 1). Looking at the spread of all reanalyses and models at 65°N shows that the TE trends in the reanalysis datasets are outside of the interquartile range of the TE trends in AMIP and coupled models (Fig. 7).

This TE trend discrepancy between models and the reanalysis datasets is likely tied to Arctic warming. Coupled CMIP6 models capture Arctic warming better than AMIP models due to a lack of change in sea ice thickness in AMIP models (Hahn et al. 2022), but they still generally underestimate observed Arctic warming since 1980 (Chylek et al. 2022). A larger amount of Arctic warming (relative to tropical warming) decreases the meridional temperature gradient and leads to less TE. This explains why the reanalyses have a larger magnitude negative TE trend than coupled simulations, while AMIP models

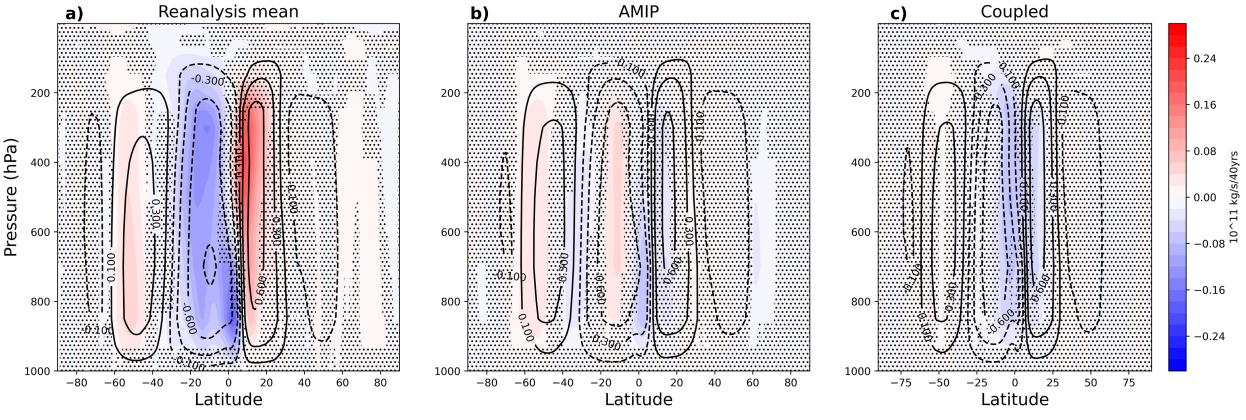

FIG. 5. Mass overturning streamfunctions for (a) the reanalyses mean, (b) the AMIP model mean, and (c) the coupled model mean. Black contours are the climatological values (contour values are labeled and are in units of 10^{11} kg s^{-1}) and the colored shading shows the 40-yr linear trend. Stippling indicates regions where the three reanalyses do not agree on the sign of the trend or, for the AMIP and coupled models, regions where less than 90% of the models agree on the sign of the trend.

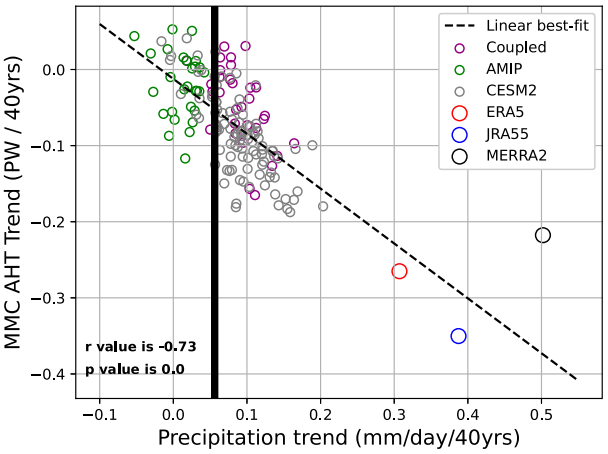

FIG. 6. Tropical precipitation trends (x axis; averaged from 10°S to 25°N) and the Southern Hemisphere tropics MMC trends (y axis; evaluated at 15°S). The vertical black line is the GPCP precipitation trend and the dashed diagonal line is the linear best-fit line with the corresponding correlation coefficient and p value in the bottom-left corner.

actually show positive TE trends (Fig. 1c). The SE trends are in better agreement between the reanalyses and models at 65°N (Fig. 7), although SE trends are larger in the reanalyses than models north of 65°N.

The second region of interest is near 50°N where there is a noticeable positive TE trend and negative SE trend in the means of the reanalysis datasets, AMIP models, and coupled models (Figs. 1c,d). However, there is considerable uncertainty surrounding these trends (Fig. 8). Two of the three reanalyses show positive TE trends at 50°N that are near or beyond the edge of the interquartile ranges of the models, but MERRA-2 shows a negative trend and AMIP and coupled models show mean trends near zero with large intermodel spread. There is generally good agreement between the reanalysis datasets and models on the negative SE trend, albeit with considerable ensemble spread (Fig. 8b).

Observations show reduced zonal-mean SST trends around 50°N (supplemental Fig. 4). Similar to our Southern Hemisphere analysis, we find that TE trends are correlated with meridional SST gradient trends in this region across all the reanalyses and coupled models (Fig. 9). However, the spread of AMIP TE trends (gray violin plot in Fig. 9) shows that even when given the observed SST pattern, models can still simulate a range of TE trends, perhaps in part due to natural variability. Additionally, we note that at these latitudes there is both significant zonal variation in the SST trends (Wills et al. 2022) and limited ocean area. While a thorough analysis of the zonal variations in SST and TE trends is beyond the scope of this study, we note that the zonal-mean SST trends at these latitudes are dominated by the Pacific Ocean SST trends given its larger size. Thus, the connections between TE trends and SST trends may be regionally specific. We also note that using surface air temperature instead of SSTs produces similar results (not shown).

A detailed exploration of seasonal trends is beyond the scope of this work, but we note that the TE trends at 50°N show substantial seasonal variation (supplemental Figs. 7a,c,d) with positive trends in winter and negative trends in summer. We also find that the SE trends and meridional SST gradients are not

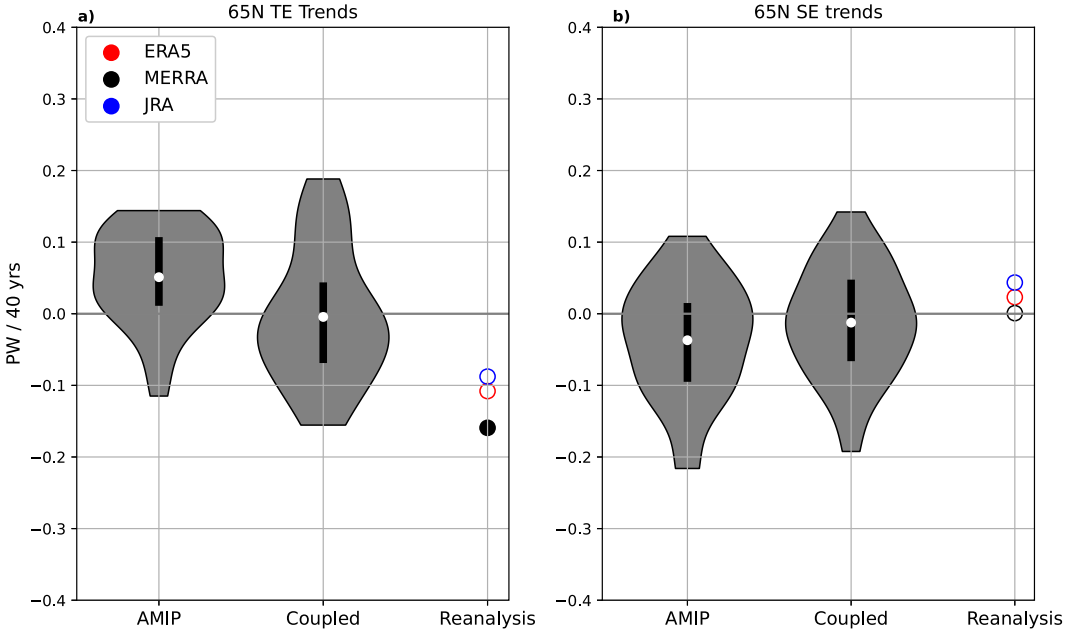

FIG. 7. Trends at 65°N for (a) TE trends and (b) SE trends for the AMIP models, coupled models, and reanalyses. For AMIP and coupled models the violin plots show the ensemble distributions, where the width of the shading indicates probability density, the thick black lines indicate the interquartile range, and the white dots indicate the mean value. For the reanalyses, filled circles denote trends that are statistically different from zero at the 95% confidence level, while open circles denote trends that are not.

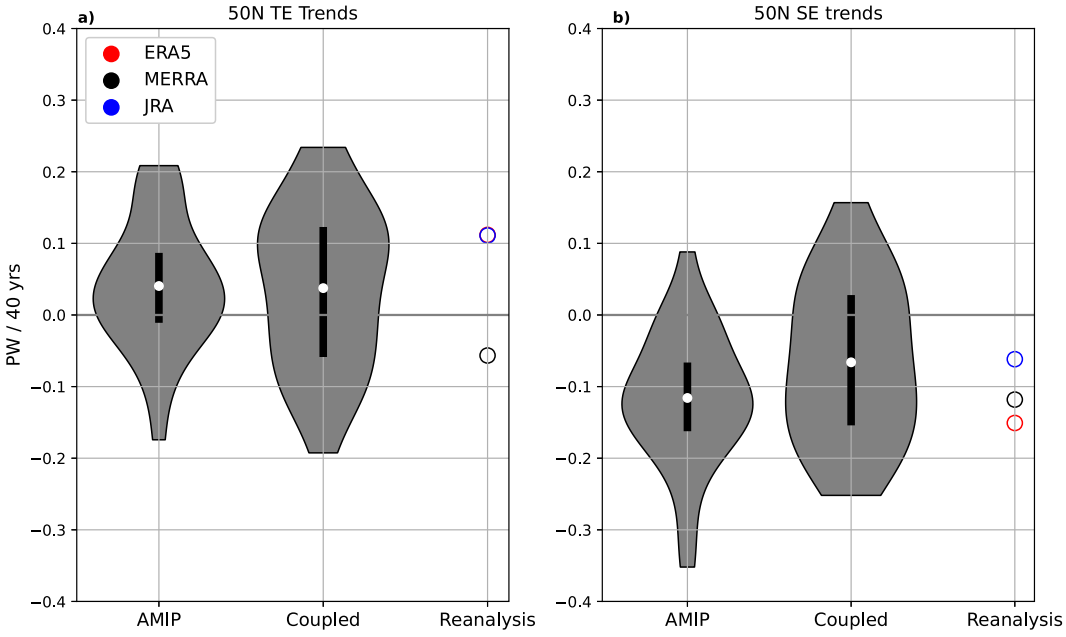

FIG. 8. Trends at 50°N for (a) TE trends and (b) SE trends for the AMIP models, coupled models, and reanalyses. For AMIP and coupled models the violin plots show the ensemble distributions, where the width of the shading indicates probability density, the thick black lines indicate the interquartile range, and the white dots indicate the mean value. For the reanalyses, filled circles denote trends that are statistically different from zero at the 95% confidence level, while open circles denote trends that are not. Note that ERA5 and JRA-55 are almost identical in (a).

well correlated (not shown), supporting previous work that found SE trends were not closely linked to meridional land temperature gradient trends (Park and Lee 2022).

d. Compensation between AHT components

Trends in individual AHT components do not happen independently; a change in one AHT component can cause changes in another. As a result, it is useful to think about the AHT system holistically and consider how all AHT components are connected.

In the previous analysis, we identified several apparent compensations between trends in different components of AHT. The first major compensation occurs between eddies (the sum of TE and SE) and the MMC. In the midlatitudes, an intensification in eddies leads to an intensification of the MMC (via Ferrel cell intensification) (e.g., Salustri and Stone 1983; Sasamori and Melgarejo 1978). The MMC and eddy climatologies in the midlatitudes are of opposite signs, so an intensification of both results in opposite signed changes. In the Southern Ocean, the trends in eddies and the MMC are opposite-signed in the ensemble means (Fig. 2) and show a strong negative correlation when all individual models and datasets are examined (Fig. 10). This same negative correlation can also be seen in the Northern Hemisphere midlatitudes (supplemental Fig. 6). In both the ensemble means and in individual models the compensation is not complete. The best-fit line in Fig. 10 shows that an eddy trend is typically compensated by an MMC trend with roughly half the magnitude. The opposite-signed changes are not only visible in the trends since 1980, but also in the interannual variability of the eddy and MMC (supplemental Fig. 8). This demonstrates that this compensation is taking place over a range of time scales.

The second major compensation occurs between SE and TE. This compensation has theoretical justification, as SE can modify the baroclinicity that TE relies on while TE and the heating associated with it can help drive SE (Branstator 1995; Chang et al. 2002; Held et al. 2002; Inatsu et al. 2002; Kaspi and Schneider 2013) and has been found in trends of AHT in individual months (Shaw et al. 2018; Park and Lee 2022). We find examples of this compensation in the Northern Hemisphere midlatitude trends of TE and SE (supplemental Fig. 5). This compensation is less evident in the Southern Hemisphere, where SE plays a smaller role. Similar to the eddy and MMC compensation, the compensation between SE and TE is not complete. A TE trend is, on average, compensated by an SE trend with roughly half the magnitude (supplemental Fig. 5). Just as for the eddy and MMC compensation, the TE and SE compensation also occurs on interannual time scales (supplemental Fig. 9). Altogether, both of these forms of compensation result in smaller trends in total AHT than in individual components in the middle and high latitudes. If individual AHT components are examined independently, this compensation can be missed.

4. Summary and conclusions

Here we analyzed AHT trends from 1980 through 2014 in three different atmospheric reanalyses, 28 AMIP models, and 31 coupled models. We found strong agreement among reanalysis datasets and models on a strengthening of the climatological

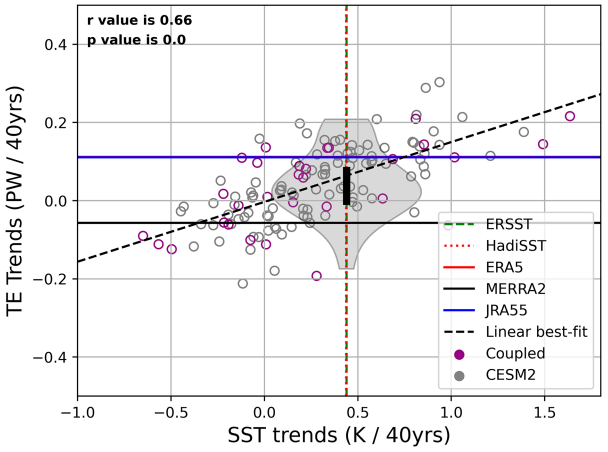

FIG. 9. Differences in SST trends between 40° and 50°N (*x* axis) and the TE trends at 50°N (*y* axis). The vertical dashed green line is the ERSSTv5 (Huang et al. 2017) estimate of the SST trends difference, the dotted red line is the HadISST SST trend estimate (Rayner et al. 2003), the horizontal lines are the TE trends from the reanalyses, and the dashed diagonal line is the linear best-fit line with the corresponding correlation coefficient and *p* value in the top-left corner. AMIP models use the HadISST dataset. Note that both the ERA5 and JRA-55 lines and HadISST and ERSST lines are mostly overlapping. Open circles denote models that have one or both of SST and TE trends that are not statistically different from zero at the 95% confidence level. The gray shading of the violin plot shows the AMIP ensemble TE trend values, where the width of the shading indicates probability density and the thick black lines indicate the interquartile range.

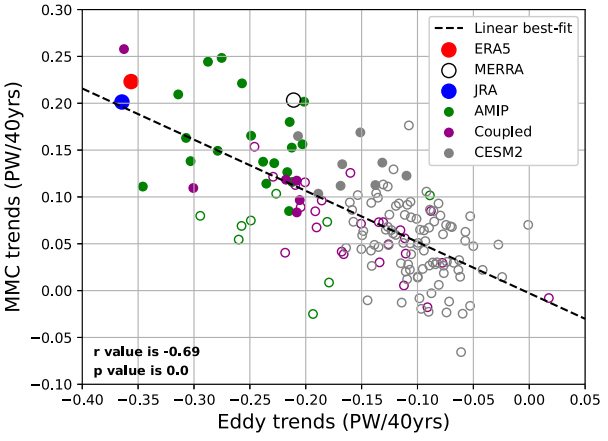

FIG. 10. Trends of eddies (*x* axis) vs trends of the MMC (*y* axis) for the three reanalyses, all the AMIP and coupled models, and for the CESM2-LENS2 ensemble. The latitudes for each point are found by finding the latitude within the 40°–60°S range with the minimum eddy trend. The MMC trend value is selected at that same latitude. The dashed diagonal line is the linear best-fit line with the corresponding correlation coefficient and *p* value in the bottom-left corner. Filled circles denote models that have both eddy and MMC trends that are statistically different from zero at the 95% confidence level, while open circles denote models that do not.

TE and MMC in the Southern Ocean. The magnitude of the reanalysis TE trends in the Southern Ocean are better captured by AMIP than coupled models due to coupled models' inaccurate simulations of SST trends in that region. These TE trends in the Southern Ocean are well compensated by opposite-signed MMC trends, resulting in smaller magnitude total AHT trends than suggested from TE trends alone. In the tropics, the reanalyses show large, and likely unreasonable, MMC trends that we find are related to larger-than-observed precipitation trends, in agreement with previous work that investigated Hadley-cell mass transports (Hu et al. 2018; Chemke and Polvani 2019; Zaplotnik et al. 2022). In the Northern Hemisphere, we find trends that are less uniform, with disagreements on the sign of trends between the reanalyses and models at many latitudes.

While trends differed region to region, a few overarching principles emerged. The first is the importance of recognizing compensations between dynamic AHT components when considering AHT trends. Considering AHT components individually will often give the wrong impression about the magnitude of total AHT changes. A second principle is the difficulty in identifying robust trends over such a short time period. In many regions there is disagreement between models and the reanalyses, or even disagreement among reanalyses. Internal variability can play a major role over a 40-yr time scale, which can introduce reanalysis–model discrepancies (Deser et al. 2020; Blackport and Fyfe 2022). There is not yet evidence of increases in total poleward AHT magnitude at most latitudes as have been projected under global warming (Hwang and Frierson 2010; Zelinka and Hartmann 2012; Armour et al. 2019).

The disagreement among reanalyses is a difficult problem to resolve. In the tropics we were able to build upon previous work (Hu et al. 2018; Chemke and Polvani 2019; Zaplotnik et al. 2022) and use precipitation trends as a way to evaluate reanalysis AHT trends in that region. However, validating each reanalysis product in every region of interest is beyond the scope of this work. Thus, we are left assuming that, outside of the tropics, each reanalysis provides an equally likely representation of AHT trends since 1980. Given the close connections that AHT has to the hydrologic cycle and to meridional temperature gradients, it is important to continue monitoring AHT trends over the coming decades.

Acknowledgments. We acknowledge support for T. C., K. C. A., A. D., and G. H. R. from National Science Foundation Award CLD2019647.

Data availability statement. All data used in this comment are publicly available reanalysis datasets. Data can be found as follows:

ERA5: https://www.ecmwf.int/en/forecasts/datasets/reanalysis-datasets/era5

ERA-Interim: https://www.ecmwf.int/en/forecasts/datasets/reanalysis-datasets/era-interim

MERRA-2: https://gmao.gsfc.nasa.gov/reanalysis/MERRA-2/

JRA: https://rda.ucar.edu/datasets/ds628.0/

CMIP6: https://pcmdi.llnl.gov/CMIP6/

CESM2: https://www.cesm.ucar.edu/community-projects/lens2/data-sets

GPCP: https://psl.noaa.gov/data/gridded/data.gpcp.html

REFERENCES

Adler, R. F., and Coauthors, 2003: The version-2 Global Precipitation Climatology Project (GPCP) monthly precipitation analysis (1979–present). *J. Hydrometeor.*, **4**, 1147–1167, https://doi.org/10.1175/1525-7541(2003)004<1147:TVGPCP>2.0.CO;2.

Alexeev, V. A., and C. H. Jackson, 2013: Polar amplification: Is atmospheric heat transport important? *Climate Dyn.*, **41**, 533–547, https://doi.org/10.1007/s00382-012-1601-z.

Armour, K. C., N. Siler, A. Donohoe, and G. H. Roe, 2019: Meridional atmospheric heat transport constrained by energetics and mediated by large-scale diffusion. *J. Climate*, **32**, 3655–3680, https://doi.org/10.1175/JCLI-D-18-0563.1.

Baggett, C., and S. Lee, 2017: An identification of the mechanisms that lead to Arctic warming during planetary-scale and synoptic-scale wave life cycles. *J. Atmos. Sci.*, **74**, 1859–1877, https://doi.org/10.1175/JAS-D-16-0156.1.

Blackport, R., and J. C. Fyfe, 2022: Climate models fail to capture strengthening winter-time North Atlantic jet and impacts on Europe. *Sci. Adv.*, **8**, eabn3112, https://doi.org/10.1126/sciadv.abn3112.

Branstator, G., 1995: Organization of storm track anomalies by recurring low-frequency circulation anomalies. *J. Atmos. Sci.*, **52**, 207–226, https://doi.org/10.1175/1520-0469(1995)052<0207:OOSTAB>2.0.CO;2.

Chang, E. K. M., S. Lee, and K. L. Swanson, 2002: Storm track dynamics. *J. Climate*, **15**, 2163–2183, https://doi.org/10.1175/1520-0442(2002)015<02163:STD>2.0.CO;2.

Chaudhuri, A. H., R. M. Ponte, G. Forget, and P. Heimbach, 2013: A comparison of atmospheric reanalysis surface products over the ocean and implications for uncertainties in air–sea boundary forcing. *J. Climate*, **26**, 153–170, https://doi.org/10.1175/JCLI-D-12-00090.1.

Chemke, R., and L. M. Polvani, 2019: Opposite tropical circulation trends in climate models and in reanalyses. *Nat. Geosci.*, **12**, 528–532, https://doi.org/10.1038/s41561-019-0383-x.

——, and ——, 2020: Linking midlatitudes eddy heat flux trends and polar amplification. *npj Climate Atmos. Sci.*, **3**, 8, https://doi.org/10.1038/s41612-020-0111-7.

——, Y. Ming, and J. Yuval, 2022: The intensification of winter mid-latitude storm tracks in the Southern Hemisphere. *Nat. Climate Change*, **12**, 553–557, https://doi.org/10.1038/s41558-022-01368-8.

Chung, E.-S., and Coauthors, 2022: Antarctic sea-ice expansion and Southern Ocean cooling linked to tropical variability. *Nat. Climate Change*, **12**, 461–468, https://doi.org/10.1038/s41558-022-01339-z.

Chylek, P., C. Folland, J. D. Klett, M. Wang, N. Hengartner, G. Lesins, and M. K. Dubey, 2022: Annual mean arctic amplification 1970–2020: Observed and simulated by CMIP6 climate models. *Geophys. Res. Lett.*, **49**, e2022GL099371, https://doi.org/10.1029/2022GL099371.

Cox, T., A. Donohoe, G. H. Roe, K. C. Armour, and D. M. W. Frierson, 2022: Near invariance of poleward atmospheric heat transport in response to midlatitude orography. *J. Climate*, **35**, 4099–4113, https://doi.org/10.1175/JCLI-D-21-0888.1.

Danabasoglu, G., and Coauthors, 2020: The Community Earth System Model version 2 (CESM2). *J. Adv. Model. Earth Syst.*, **12**, e2019MS001916, https://doi.org/10.1029/2019MS001916.

Deser, C., and Coauthors, 2020: Insights from Earth system model initial-condition large ensembles and future prospects. *Nat. Climate Change*, **10**, 277–286, https://doi.org/10.1038/s41558-020-0731-2.

Dong, Y., and Coauthors, 2021: Biased estimates of equilibrium climate sensitivity and transient climate response derived from historical CMIP6 simulations. *Geophys. Res. Lett.*, **48**, e2021GL095778, https://doi.org/10.1029/2021GL095778.

Donohoe, A., K. C. Armour, G. H. Roe, D. S. Battisti, and L. Hahn, 2020: The partitioning of meridional heat transport from the last glacial maximum to CO_2 quadrupling in coupled climate models. *J. Climate*, **33**, 4141–4165, https://doi.org/10.1175/JCLI-D-19-0797.1.

Eyring, V., S. Bony, G. A. Meehl, C. A. Senior, B. Stevens, R. J. Stouffer, and K. E. Taylor, 2016: Overview of the Coupled Model Intercomparison Project phase 6 (CMIP6) experimental design and organization. *Geosci. Model Dev.*, **9**, 1937–1958, https://doi.org/10.5194/gmd-9-1937-2016.

Fajber, R., A. Donohoe, S. Ragen, K. C. Armour, and P. J. Kushner, 2023: Atmospheric heat transport is governed by meridional gradients in surface evaporation in modern-day earth-like climates. *Proc. Natl. Acad. Sci. USA*, **120**, e2217202120, https://doi.org/10.1073/pnas.2217202120.

Gelaro, R., and Coauthors, 2017: The Modern-Era Retrospective Analysis for Research and Applications, version 2 (MERRA-2). *J. Climate*, **30**, 5419–5454, https://doi.org/10.1175/JCLI-D-16-0758.1.

Grytsai, A. V., O. M. Evtushevsky, O. V. Agapitov, A. R. Klekociuk, and G. P. Milinevsky, 2007: Structure and long-term change in the zonal asymmetry in Antarctic total ozone during spring. *Ann. Geophys.*, **25**, 361–374, https://doi.org/10.5194/angeo-25-361-2007.

Gu, G., R. F. Adler, and G. J. Huffman, 2016: Long-term changes/trends in surface temperature and precipitation during the satellite era (1979–2012). *Climate Dyn.*, **46**, 1091–1105, https://doi.org/10.1007/s00382-015-2634-x.

Hahn, L. C., K. C. Armour, M. D. Zelinka, C. M. Bitz, and A. Donohoe, 2021: Contributions to polar amplification in CMIP5 and CMIP6 models. *Front. Earth Sci.*, **9**, 710036, https://doi.org/10.3389/feart.2021.710036.

——, ——, D. S. Battisti, I. Eisenman, and C. M. Bitz, 2022: Seasonality in Arctic warming driven by sea ice effective heat capacity. *J. Climate*, **35**, 1629–1642, https://doi.org/10.1175/JCLI-D-21-0626.1.

Hassler, B., and A. Lauer, 2021: Comparison of reanalysis and observational precipitation datasets including ERA5 and WFDE5. *Atmosphere*, **12**, 1462, https://doi.org/10.3390/atmos12111462.

Held, I. M., 1999: The macroturbulence of the troposphere. *Tellus*, **51A**, 59–70, https://doi.org/10.3402/tellusa.v51i1.12306.

——, and B. J. Soden, 2006: Robust responses of the hydrological cycle to global warming. *J. Climate*, **19**, 5686–5699, https://doi.org/10.1175/JCLI3990.1.

——, M. Ting, and H. Wang, 2002: Northern winter stationary waves: Theory and modeling. *J. Climate*, **15**, 2125–2144, https://doi.org/10.1175/1520-0442(2002)015<2125:NWSWTA>2.0.CO;2.

Hersbach, H., and Coauthors, 2020: The ERA5 global reanalysis. *Quart. J. Roy. Meteor. Soc.*, **146**, 1999–2049, https://doi.org/10.1002/qj.3803.

Holton, J. R., and D. O. Staley, 1973: An introduction to dynamic meteorology. *Amer. J. Phys.*, **41**, 752–754, https://doi.org/10.1119/1.1987371.

Hu, Y., H. Huang, and C. Zhou, 2018: Widening and weakening of the Hadley circulation under global warming. *Sci. Bull.*, **63**, 640–644, https://doi.org/10.1016/j.scib.2018.04.020.

Huang, B., and Coauthors, 2017: Extended Reconstructed Sea Surface Temperature, version 5 (ERSSTv5): Upgrades, validations, and intercomparisons. *J. Climate*, **30**, 8179–8205, https://doi.org/10.1175/JCLI-D-16-0836.1.

Hurrell, J. W., J. J. Hack, D. Shea, J. M. Caron, and J. Rosinski, 2008: A new sea surface temperature and sea ice boundary dataset for the Community Atmosphere Model. *J. Climate*, **21**, 5145–5153, https://doi.org/10.1175/2008JCLI2292.1.

Hwang, Y.-T., and D. M. W. Frierson, 2010: Increasing atmospheric poleward energy transport with global warming. *Geophys. Res. Lett.*, **37**, L24807, https://doi.org/10.1029/2010GL045440.

Inatsu, M., H. Mukougawa, and S.-P. Xie, 2002: Stationary eddy response to surface boundary forcing: Idealized GCM experiments. *J. Atmos. Sci.*, **59**, 1898–1915, https://doi.org/10.1175/1520-0469(2002)059<1898:SERTSB>2.0.CO;2.

Ivanciu, I., K. Matthes, S. Wahl, J. Harlaß, and A. Biastoch, 2021: Effects of prescribed CMIP6 ozone on simulating the Southern Hemisphere atmospheric circulation response to ozone depletion. *Atmos. Chem. Phys.*, **21**, 5777–5806, https://doi.org/10.5194/acp-21-5777-2021.

Kapsch, M.-L., R. G. Graversen, and M. Tjernström, 2013: Springtime atmospheric energy transport and the control of Arctic summer sea-ice extent. *Nat. Climate Change*, **3**, 744–748, https://doi.org/10.1038/nclimate1884.

Kaspi, Y., and T. Schneider, 2013: The role of stationary eddies in shaping midlatitude storm tracks. *J. Atmos. Sci.*, **70**, 2596–2613, https://doi.org/10.1175/JAS-D-12-082.1.

Kim, J.-E., and M. J. Alexander, 2013: Tropical precipitation variability and convectively coupled equatorial waves on submonthly time scales in reanalyses and TRMM. *J. Climate*, **26**, 3013–3030, https://doi.org/10.1175/JCLI-D-12-00353.1.

Kobayashi, S., and Coauthors, 2015: The JRA-55 reanalysis: General specifications and basic characteristics. *J. Meteor. Soc. Japan*, **93**, 5–48, https://doi.org/10.2151/jmsj.2015-001.

Lavers, D. A., A. Simmons, F. Vamborg, and M. J. Rodwell, 2022: An evaluation of ERA5 precipitation for climate monitoring. *Quart. J. Roy. Meteor. Soc.*, **148**, 3152–3165, https://doi.org/10.1002/qj.4351.

Liu, H., Z. Song, X. Wang, and V. Misra, 2022: An ocean perspective on CMIP6 climate model evaluations. *Deep-Sea Res. II*, **201**, 105120, https://doi.org/10.1016/j.dsr2.2022.105120.

Marshall, J., A. Donohoe, D. Ferreira, and D. McGee, 2014: The ocean's role in setting the mean position of the inter-tropical convergence zone. *Climate Dyn.*, **42**, 1967–1979, https://doi.org/10.1007/s00382-013-1767-z.

Park, M., and S. Lee, 2019: Relationship between tropical and extratropical diabatic heating and their impact on stationary–transient wave interference. *J. Atmos. Sci.*, **76**, 2617–2633, https://doi.org/10.1175/JAS-D-18-0371.1.

——, and ——, 2022: On the causes of synoptic-scale eddy heat flux decline. *Geophys. Res. Lett.*, **49**, e2022GL100963, https://doi.org/10.1029/2022GL100963.

Pierrehumbert, R. T., 2010: *Principles of Planetary Climate*. Cambridge University Press, 674 pp.

Ramaswamy, V., M. D. Schwarzkopf, and W. J. Randel, 1996: Fingerprint of ozone depletion in the spatial and temporal pattern of recent lower-stratospheric cooling. *Nature*, **382**, 616–618, https://doi.org/10.1038/382616a0.

Randel, W. J., and F. Wu, 1999: Cooling of the Arctic and Antarctic polar stratospheres due to ozone depletion. *J. Climate*, **12**, 1467–1479, https://doi.org/10.1175/1520-0442(1999)012<1467:COTAAA>2.0.CO;2.

Rayner, N. A., D. E. Parker, E. B. Horton, C. K. Folland, L. V. Alexander, D. P. Rowell, E. C. Kent, and A. Kaplan, 2003: Global analyses of sea surface temperature, sea ice, and night marine air temperature since the late nineteenth century. *J. Geophys. Res.*, **108**, 4407, https://doi.org/10.1029/2002JD002670.

Rodgers, K. B., and Coauthors, 2021: Ubiquity of human-induced changes in climate variability. *Earth Syst. Dyn.*, **12**, 1393–1411, https://doi.org/10.5194/esd-12-1393-2021.

Salustri, G., and P. H. Stone, 1983: A diagnostic study of the forcing of the Ferrel cell by eddies, with latent heat effects included. *J. Atmos. Sci.*, **40**, 1101–1109, https://doi.org/10.1175/1520-0469(1983)040<1101:ADSOTF>2.0.CO;2.

Sasamori, T., and J. Melgarejo, 1978: A parameterization of large-scale heat transport in mid-latitudes. Part I. Transient eddies. *Tellus*, **30** (4), 289–299.

Shaw, T. A., P. Barpanda, and A. Donohoe, 2018: A moist static energy framework for zonal-mean storm-track intensity. *J. Atmos. Sci.*, **75**, 1979–1994, https://doi.org/10.1175/JAS-D-17-0183.1.

——, O. Miyawaki, and A. Donohoe, 2022: Stormier Southern Hemisphere induced by topography and ocean circulation. *Proc. Natl. Acad. Sci. USA*, **119**, e2123512119, https://doi.org/10.1073/pnas.2123512119.

Siler, N., G. H. Roe, and K. C. Armour, 2018: Insights into the zonal-mean response of the hydrologic cycle to global warming from a diffusive energy balance model. *J. Climate*, **31**, 7481–7493, https://doi.org/10.1175/JCLI-D-18-0081.1.

Sun, Q., C. Miao, Q. Duan, H. Ashouri, S. Sorooshian, and K.-L. Hsu, 2018: A review of global precipitation data sets: Data sources, estimation, and intercomparisons. *Rev. Geophys.*, **56**, 79–107, https://doi.org/10.1002/2017RG000574.

Thompson, D. W. J., and S. Solomon, 2002: Interpretation of recent Southern Hemisphere climate change. *Science*, **296**, 895–899, https://doi.org/10.1126/science.1069270.

Trenberth, K. E., and D. P. Stepaniak, 2003: Seamless poleward atmospheric energy transports and implications for the Hadley circulation. *J. Climate*, **16**, 3706–3722, https://doi.org/10.1175/1520-0442(2003)016<3706:SPAETA>2.0.CO;2.

——, J. T. Fasullo, and J. Kiehl, 2009: Earth's global energy budget. *Bull. Amer. Meteor. Soc.*, **90**, 311–324, https://doi.org/10.1175/2008BAMS2634.1.

Walker, C. C., and T. Schneider, 2006: Eddy influences on Hadley circulations: Simulations with an idealized GCM. *J. Atmos. Sci.*, **63**, 3333–3350, https://doi.org/10.1175/JAS3821.1.

Wild, M., D. Folini, C. Schär, N. Loeb, E. G. Dutton, and G. König-Langlo, 2013: The global energy balance from a surface perspective. *Climate Dyn.*, **40**, 3107–3134, https://doi.org/10.1007/s00382-012-1569-8.

——, and Coauthors, 2015: The energy balance over land and oceans: An assessment based on direct observations and CMIP5 climate models. *Climate Dyn.*, **44**, 3393–3429, https://doi.org/10.1007/s00382-014-2430-z.

Wills, R. C. J., Y. Dong, C. Proistosecu, K. C. Armour, and D. S. Battisti, 2022: Systematic climate model biases in the large-scale patterns of recent sea-surface temperature and sea-level pressure change. *Geophys. Res. Lett.*, **49**, e2022GL100011, https://doi.org/10.1029/2022GL100011.

Woods, C., and R. Caballero, 2016: The role of moist intrusions in winter Arctic warming and sea ice decline. *J. Climate*, **29**, 4473–4485, https://doi.org/10.1175/JCLI-D-15-0773.1.

——, ——, and G. Svensson, 2013: Large-scale circulation associated with moisture intrusions into the Arctic during winter. *Geophys. Res. Lett.*, **40**, 4717–4721, https://doi.org/10.1002/grl.50912.

Zaplotnik, Ž., M. Pikovnik, and L. Boljka, 2022: Recent Hadley circulation strengthening: A trend or multidecadal variability? *J. Climate*, **35**, 4157–4176, https://doi.org/10.1175/JCLI-D-21-0204.1.

Zelinka, M. D., and D. L. Hartmann, 2012: Climate feedbacks and their implications for poleward energy flux changes in a warming climate. *J. Climate*, **25**, 608–624, https://doi.org/10.1175/JCLI-D-11-00096.1.